The influence of probe spacing and probe bias in a double Langmuir probe setup

Cite as: AIP Advances 11, 085007 (2021); doi: 10.1063/5.0058540
Submitted: 31 May 2021 • Accepted: 21 July 2021 •
Published Online: 3 August 2021

Kai Morgan Kjølerbakken,[1,2,a)] Wojciech J. Miloch,[1] and Ketil Røed[1]

AFFILIATIONS

[1] Department of Physics, University of Oslo, Oslo 0316, Norway
[2] Norwegian Institute for Air Research, Kjeller 2007, Norway

[a)] **Author to whom correspondence should be addressed:** kaimk@fys.uio.no

ABSTRACT

Multi-needle Langmuir probes are mounted on satellites and sounding rockets for high-frequency characterization of plasma in the ionosphere. Mounted on a spacecraft, the recorded probe current often differs from expected results. In this paper, we perform a numerical study using a particle in cell model to see how the spacing between the individual probes used in a multi-needle setup influences the measured current. We also study how the applied probe bias voltage can contribute to deviations. In our study, we use realistic electron temperatures and electron densities for the relevant part of the ionosphere. However, the results should be generally applicable and valid for other space environments as well as for laboratory Langmuir probe applications. From our study, we can see that when the distance is short, less than two Debye lengths, the current is highly affected, and we can see deviations of more than 60% compared to a single probe setup.

I. INTRODUCTION

The interaction between plasma and solid objects, such as rockets, satellites, probes, moons, asteroids, or dust grains, remains one of the main problems in plasma and space physics.[1,2] Since their introduction by Mott-Smith and Langmuir in the 1920s,[3] Langmuir probes have been widely adapted for characterization of plasma. They were initially used for plasma chamber diagnostics and were later adapted for space applications.[4] Langmuir probes are now the preferred instrument for *in situ* characterization of plasma in space where they typically perform a measurement locally in the vicinity of a satellite or spacecraft. A Langmuir probe is basically an electrode that is immersed into plasma. The current, which is the sum of the collected electrons and ions, is measured as a function of the applied bias voltage to the probe, which produces a current–voltage graph that is used to extract plasma parameters as density and temperature. The traditional approach to perform a measurement is to sweep the probe bias through a voltage range.[5] However, the plasma needs time to adjust and stabilize as the bias is changing, and this will put limitations on the sweeping frequency and again on the temporal resolution.[6]

For a satellite in a low Earth orbit, the speed is about 7.8 km/s, and a high sampling rate is required to give a meaningful spatial resolution sufficient to know if the measured values are caused by the change in location or actual changes caused by waves or fluctuations in the plasma. To achieve higher sampling frequency, a multi-Needle Langmuir Probe (m-NLP) setup has been developed.[7] Two or more Langmuir probes were utilized, each with their own fixed bias that reduces the time that the probes need to stabilize and allows a much higher sampling rate. In space applications, the recorded probe current from an m-NLP system often differs from expected results, and in an m-NLP setup, it is natural to assume that when two probes get close to each other, they will mutually interfere with each other and compromise the measurements. It has been shown that two probes can generate a common sheath when the distance separating the probes becomes small[8] and that an asymmetric bias voltage must be handled with care.[9] It is, therefore, essential to get a better understanding of how the distance separating the probes and the applied bias voltage changes the sheath effects and influences the measured current.

In this paper, we simulate and evaluate probe configurations with various spacings between the probes and various applied probe biases to see how these parameters affect the sheath and the collected probe current. Simulations are carried out using a particle in cell (PIC) model in an environment that reflects a typical low Earth orbit environment at an altitude of about 400 km. However,

the results should be generally applicable and valid for other space environments as well as for laboratory Langmuir probe applications. The paper is organized in the following manner: In Sec. II, we give an introduction to shielding effects before we introduce the theory behind for probe current. We then present the numerical study and results for the selected cases. Finally, we present a summary with concluding remarks.

II. THEORY

A. Shielding effects and biasing

When an object, and in this case a Langmuir probe, is immersed into plasma, the thermal electron flux hitting the surface of the probe will be much larger than the corresponding ion flux hitting the surface. As a result, the probe will be charged and obtain a negative potential, which generates a sheath around the probe where electrons are being repelled and positive ions are attracted. The system will reach a steady state condition, referred to as the floating potential, where the electrons and ions are balanced and the net current to the probe is equal to zero. We can control whether electrons or ions are repelled or attracted by applying a bias voltage to the probe. If the bias voltages are below the floating potential, we are in the ion saturation region where no ions are repelled. When the bias voltage is equal to the plasma potential, no sheaths exist, and all the thermal flux of electrons is collected. If the bias is between the floating potential and the plasma potential, we are in an electron retardation region where electrons are repelled by the sheath effects. When the bias voltage is further increased above the plasma potential, we enter the region referred to as the electron saturation region where no electrons are repelled. Figure 1 illustrates the voltage current characteristics of a cylindrical probe.

B. Debye length

The Debye length is a function of the thermal energy for the particles and the supersonic speed of the ions. However, since the mobility of the electrons is much higher than that of the ions, in flowing plasmas, we can in general relate the characteristic shielding to the electron Debye length,[10]

$$\lambda_D = \sqrt{\frac{k\varepsilon_0 T_e}{e^2 n_e}}, \tag{1}$$

where k is Boltzmann's constant, ε_0 is the permittivity of free space, T_e is the electron temperature, e is the electron charge, and n_e is the plasma electron density. We can see that λ_D increases with increasing thermal energy kT_e, and it decreases with increasing density n_e.

In the F-layer in the upper ionosphere, the electron temperature is relatively stable in the range 1200–1250 K. However, the electron density varies within this layer from 10^4 to 10^6 cm^3. Table I shows typical values for the Debye length in different layers in the ionosphere. The thermal speed of the electrons, roughly in the range 170–350 km s^{-1}, exceeds the speed of the rocket, typically 5–10 km s^{-1}, and the velocity of the bulk plasma, which is a few km s^{-1}.

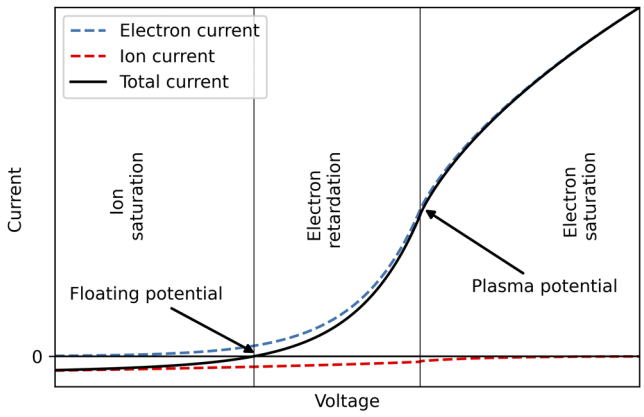

FIG. 1. Voltage current curve for a Langmuir probe, showing the floating potential V_f and the plasma potential V_p.

C. Probe biasing

When operating the probes, they will be biased relative to the floating potential of the spacecraft. This can be accomplished in two different ways: either in a fixed-bias mode or a swept-bias mode. In a swept-bias mode, the voltage sweeps through a voltage range, typically from −10 to +10 V. On a fast moving spacecraft, a swept bias mode cannot be performed fast enough to obtain the desired spatial resolution when the spacecraft is moving at 1–2 km s^{-1}, and instead, a multi-needle system with fixed probe biases is required.[7] An m-NLP setup depends on a linear assumption of the V–I^2 curve and the probes biased in the electron saturation region. It is recommended that more than two probes be used, and it is therefore common to see an m-NLP setup with three or four Langmuir probes.[11] A multi-needle setup also has several additional advantages, such as detecting if the reference potential falls too low or if the Debye length falls too low. This reduces the chance of errors and increases the robustness of the method.[7]

D. Probe current

The probe current is given by the sum of the incoming charged ions and electrons and depends on the temperature and the particle density. However, to estimate the current, we also need to take into account the geometry of the probe, commonly divided into the three categories—plane, spherical, and cylindrical probes—as seen in Fig. 2. Analytic solutions for the probe current for each of these three shapes were derived by Langmuir and Mott-Smith and are referred to as Orbital Motion Limited (OML) theory.[3] The current I_c for a cylindrical probe operated in the electron saturation region is given by

TABLE I. Typical Debye lengths for different layers in the ionosphere.

Layer	D	E	F
Electron density (cm^{-3})	100	10^5	10^6
Electron temperature (K)	600	900	1200
Electron Debye-length (mm)	~ 170	~ 7	~ 2

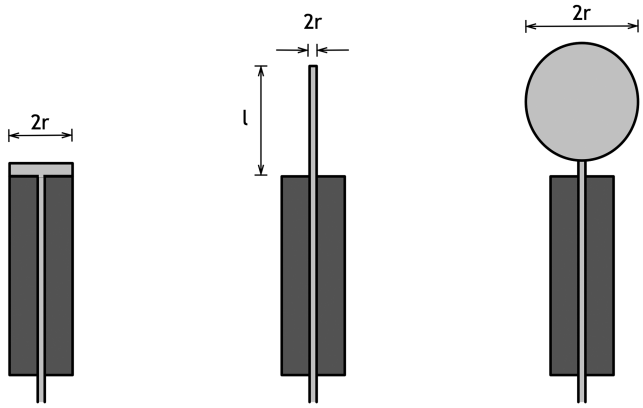

FIG. 2. Illustration of a planar, cylindrical, and spherical Langmuir probe.

$$I_c = CI_{th}\left(1 + \frac{eV}{kT_e}\right)^{\beta}, \tag{2}$$

where

$$I_{th} = n_e e\sqrt{\frac{kT_e}{2\pi m_e}}A, \tag{3}$$

where m_e is the electron mass, r is the cylinder radius, l is the cylinder length, and V is the probe potential with respect to ground. For a cylindrical probe, $C = \frac{2}{\sqrt{\pi}}$, and for a spherical probe, $C = 1$. A is the surface area of the probe. For a cylindrical probe with an infinite length, β is equal to 0.5. This expression for the current is valid for a collisionless, non-drifting, Maxwellian distributed and non-magnetized plasma. In this study, we focus on probes with a cylindrical geometry where the geometry must fulfill the following criteria: The probe itself must be very thin compared to the Debye length ($r \ll \lambda_D$), and the length of the probe must be very long compared to the Debye length ($l \gg \lambda_D$), thereby also neglecting parallel motion along the probe as well as neglecting the end effects of the probe. However, in practice, the length of the probe and edge effects need to be accounted for, and β should be fitted empirically to values between 0.5 and 1.[12,13]

E. *In situ* m-NLP measurements

The sheath effects depend on the size of the probe, and it is desirable to make the probes as small as possible to reduce these effects. The disadvantage is that a small probe collects fewer particles and generates a lower current, which is noisier and harder to measure. The Langmuir probe in a typical m-NLP setup is a cylindrical probe and has a length in the range of 25–50 mm and a diameter of about 0.5 mm. The probes are typically made from a coaxial cable where a short insulation area is kept after the braid to avoid a short circuit between the braid and the center conductor. When a bias voltage has been applied to the probe, the probe needs some time to stabilize before the corresponding current is measured. In space, the biased voltage is relative to the spacecraft, which is also exposed to the plasma and has an unknown floating potential, and knowing the exact bias potential can be challenging.[12] A detailed description of the multi-needle Langmuir probe concept can be found in Refs. 7 and 14.

III. METHOD

Plasma simulations are commonly divided into two main classes: kinetic and fluid based methods. To obtain the appropriate spatial resolution when simulating the interaction between Langmuir probes and the surrounding plasma, a kinetic simulation model is required. The kinetic particle-in-cell (PIC) method was developed in the late 1950s and soon became a widely adopted method in plasma physics. It is an effective method for solving a kinetic particle system by solving a set of differential equations commonly referred to as the PIC cycle. The PIC cycle is a four step process[15] comprising the following steps: (1) Calculating the electric and magnetic field by solving Maxwell's equations. (2) Calculating the particle acceleration by the Lorentz force. (3) Moving the particles and updating the positions and the velocities for each particle. (4) Calculating the plasma current and charge density from the positions and velocities. The computational volume of a PIC model is a spatial grid where the particles are distributed within the cells. While a direct kinetic approach based on a one to one interaction operates at a run time of $O(N_p^2)$ for N_p particles, the PIC method dramatically reduces the computational cost by mapping the current and charge contributions into a cell structure on N_c number of cells, which runs at the order of $O(N_p)$. The field solver in the PIC cycle runs an $O(N_c \log N_c)$, and the total order of the PIC model is $O(N_p + N_c \log N_c)$.[16] The PIC model further reduces the computational cost by representing real particles with "super particles." Each super particle represents a number of real particles, and the ratio between super particles and real particles is referred to as the specific weight.

A. Simulation tools

The numerical study was accomplished with the PTetra model. PTetra is a PIC model working on an unstructured grid following a standard PIC scheme.[17,18] The geometry and mesh were generated using the meshing tool Gmsh,[19] and Fig. 3 shows the mesh of one of the simulated dual probe configurations using a cylinder as the outer boundary. Particles are initiated with Boltzmann distributed velocities given by the ion and electron temperature. The particles move in the defined volume by integrating the Lorentz force implemented as a leap frog scheme, giving second-order accuracy. The PTetra model supports static magnetic fields. However, in this study, the magnetic field effects are not considered.

B. Stability criteria

For each time-step, it is required that the change in position Δx is resolved within the Debye length: $\Delta x < \lambda_D$. Otherwise, the plasma can experience instability and artificial heating.[15,20] In addition, the temporal resolution is restricted by the size of the cell, so no particle travels more than the length of one grid cell within a single time-step. The spatial scale of objects must also be resolved,[21] and since the PTetra model uses an unstructured grid, the objects only need to be resolved locally. The PTetra model automatically computes the time-step where it accounts for the change in speed and energy due to the acceleration caused by the biased probes. However, we should

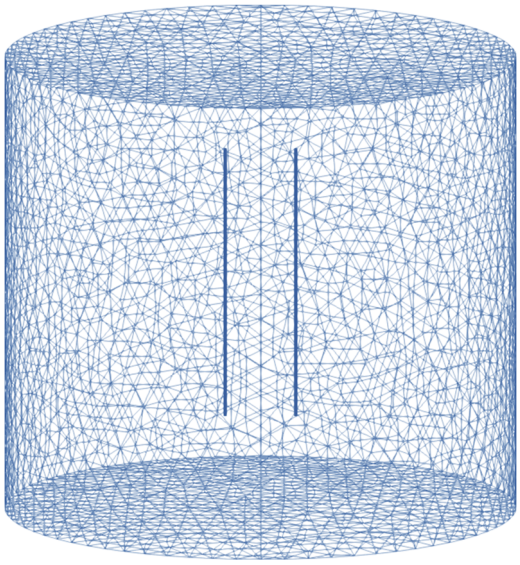

FIG. 3. Dual Langmuir probe setup within the computational volume given by a cylindrical boundary with a radius of 7 Debye lengths and spacing between the probes of two Debye lengths. Both probes have a length of 50 mm and a diameter of 0.5 mm with a flat top and bottom. In the simulations, the spacing between the two probes ranged from half the Debye length to four times the Debye length. The mesh was generated using Gmsh, with the outer mesh resolution set to 3.5 mm and the inner resolution set to 0.085 mm.

be aware that the highest resolution will be near the probe where the electric potential also is highest, resulting in the highest acceleration and velocity.

C. Boundary conditions

In the model, the outer boundary will be a Dirichlet boundary where the potential will be zero, and it is therefore important that the distance from each probe out to the outer boundary is sufficient. In the model, injection of new particles is also carried out at the outer boundary. For each time-step, the model accounts for the loss of particles by injecting new particles to keep the plasma consistent with the expected plasma conditions outside the outer boundary.

IV. NUMERICAL STUDY

The selected simulation parameters are chosen to represent a typical low Earth orbit environment at an altitude of 400 km and are carried out in quasineutral plasma where the density of the ions equals the density of the electrons. The ions are all taken to be O^+ at the same temperature and density as the electrons. We also assume a non-magnetized and non-drifting plasma. In order to reduce simulation time, we minimized the computational volume by selecting parameters that resulted in a small Debye length while still being representable for the F-region in the ionosphere. In this study, we used an electron temperature of 0.08 eV (928 K) and a density of 10^5 cm^{-3}, which in turn give a Debye length of 6.65 mm. The length of the simulated probes was 50 mm, and the diameter was 0.5 mm. The computational volume was given by a cylinder with a radius of $7\lambda_D$ and a height of 80 mm. Simulation parameters are listed in Table II. To ensure stability when changing positions of the probes from the center toward the outer boundary of the computational volume, two initial tests were run. In the first test, we used a single

TABLE II. Simulation parameters.

Parameter		Value
Electron density	n_e	10^5 cm^{-3}
Ion density	n_i	10^5 cm^{-3}
Electron temperature	T_e	0.08 eV to 928 K
Ion temperature	T_i	0.08 eV to 928 K
Electron plasma period	$2\pi\omega_{pe}^{-1}$	0.35 μs
Ion plasma period	$2\pi\omega_{pe}^{-1}$	60.1 μs
Debye length	λ_D	6.65 mm

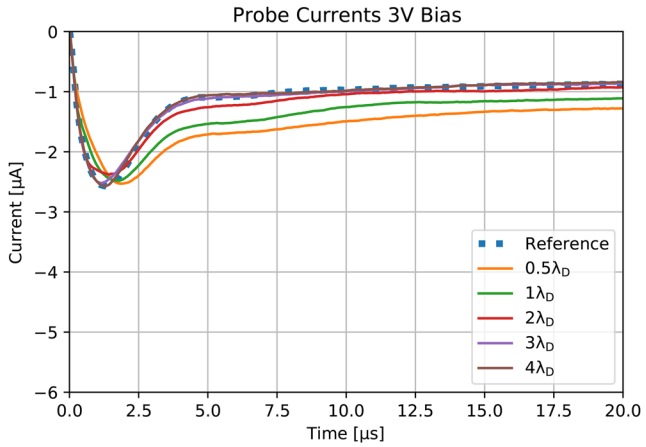

FIG. 4. Collected current of a probe biased at 3 V next to a probe biased at 0 V. The probe spacing ranges from 0.5 to 4 times the Debye length.

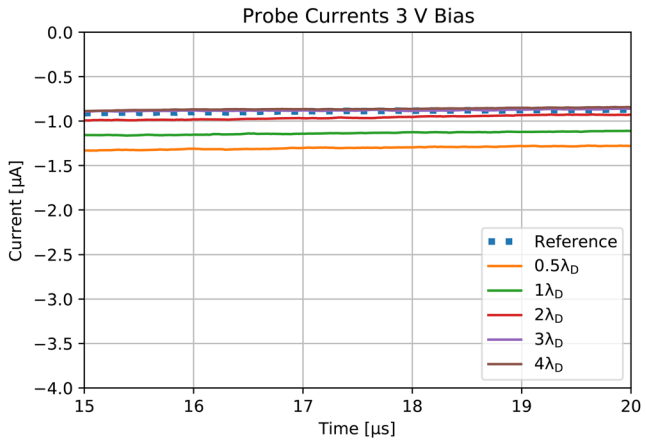

FIG. 5. The same current as in Fig. 4 for a probe biased at 3 V next to a probe biased at 0 V after reaching steady state.

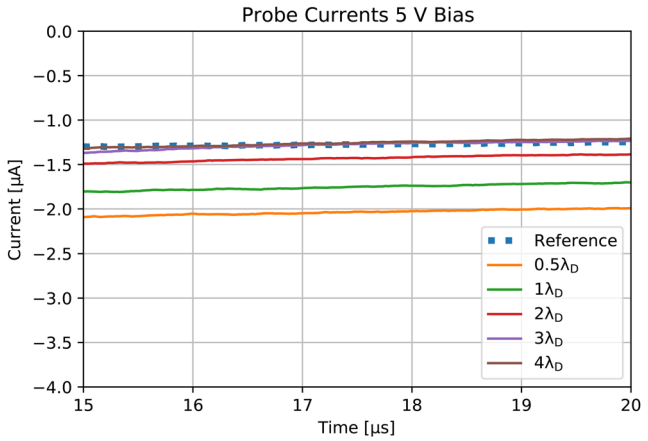

FIG. 6. Current collected by a probe biased at 5 V next to a probe biased at 0 V at steady state.

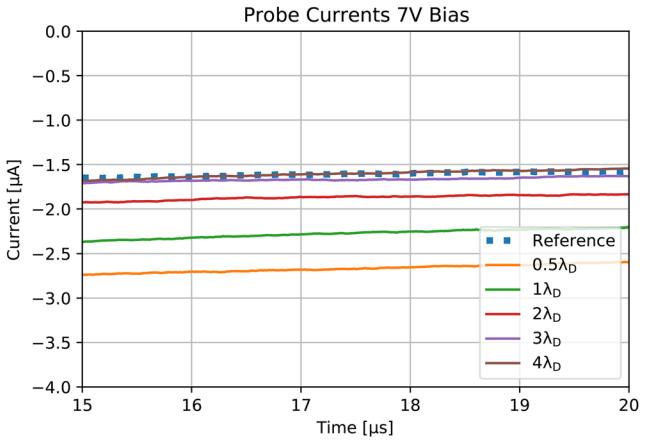

FIG. 7. Probe current of a probe biased at 7 V next to a probe biased at 0 V after reaching steady state condition.

probe that was moved from the center to outside in steps of $1\lambda_D$. This test showed that the current was stable and the equipotential was preserved up to $3\lambda_D$ off-center. This equals a probe spacing of $6\lambda_D$, well beyond the maximum spacing of $4\lambda_D$ used in the simulations. The second test was to move a dual probe setup from the center toward the outer boundary with a fixed spacing between the probes of $2\lambda_D$ and both probes biased at 5 V. This also produced comparable currents for both probes out to $3\lambda_D$ off the center. For larger distances $4\lambda_D$ and $5\lambda_D$, we could see a small increase in the current. To be sure, none of the probes were moved further out than $2\lambda_D$ off the center, always keeping a distance of more than $4.5\lambda_D$ to the outer cylinder wall boundary, while the tip of the probe was $2.25\lambda_D$ above and beneath the top and the bottom of the boundary, respectively.

We wanted to examine how the electron current to the Langmuir probe was disturbed by introducing a secondary probe

TABLE III. Currents for varying spacing. The first probe was biased at 3, 5, and 7 V next to the second probe biased at 0 V. Probe spacings range from $\lambda_D = 0.5$ to $\lambda_D = 4$. The currents are compared to the single reference probe biased at the same voltages (3, 5, and 7 V).

Probe spacing	$0.5\lambda_D$	$1\lambda_D$	$2\lambda_D$	$3\lambda_D$	$4\lambda_D$	References
Current at 3 V (μA)	−1.30	−1.13	−0.96	−0.88	−0.86	−0.89
Deviation at 3 V (%)	+45.8	+27.5	+7.8	−1.2	−2.9	
Current at 5 V (μA)	−2.03	−1.75	−1.43	−1.28	−1.26	−1.28
Deviation at 5 V (%)	+59.0	+37.0	+12.0	0.1	−1.2	
Current at 7 V (μA)	−2.64	−2.25	−1.86	−1.66	−1.59	−1.60
Deviation at 7 V (%)	+65.1	+40.6	+16.0	+3.7	−0.7	

TABLE IV. Currents for varying bias. The first probe was biased at 3, 5, and 7 V next to the second probe biased at 3, 5, and 7 V, respectively. The currents are compared to the currents of a single probe at the same voltages (3, 5, and 7 V). The probe spacing was fixed at $2\lambda_D$.

Bias second probe	$0V$	$3V$	$5V$	$7V$	References
Probe current at 3 V (μA)	−0.97	−1.24	−1.22	−1.8	−0.90
Deviation at 3 V (%)	+7.5	+37.6	+35.1	+30.6	
Current at 5 V (μA)	−1.44.	−1.85	−1.72	−1.63	−1.28
Deviation at 5 V (%)	+12.2	+44.5	+34.3	+27.4	
Current at 7 V (μA)	−1.87.	−2.30	−2.34	−2.16	−1.61
Deviation at 7 V (%)	+16.0	+42.5	+44.9	+33.8	

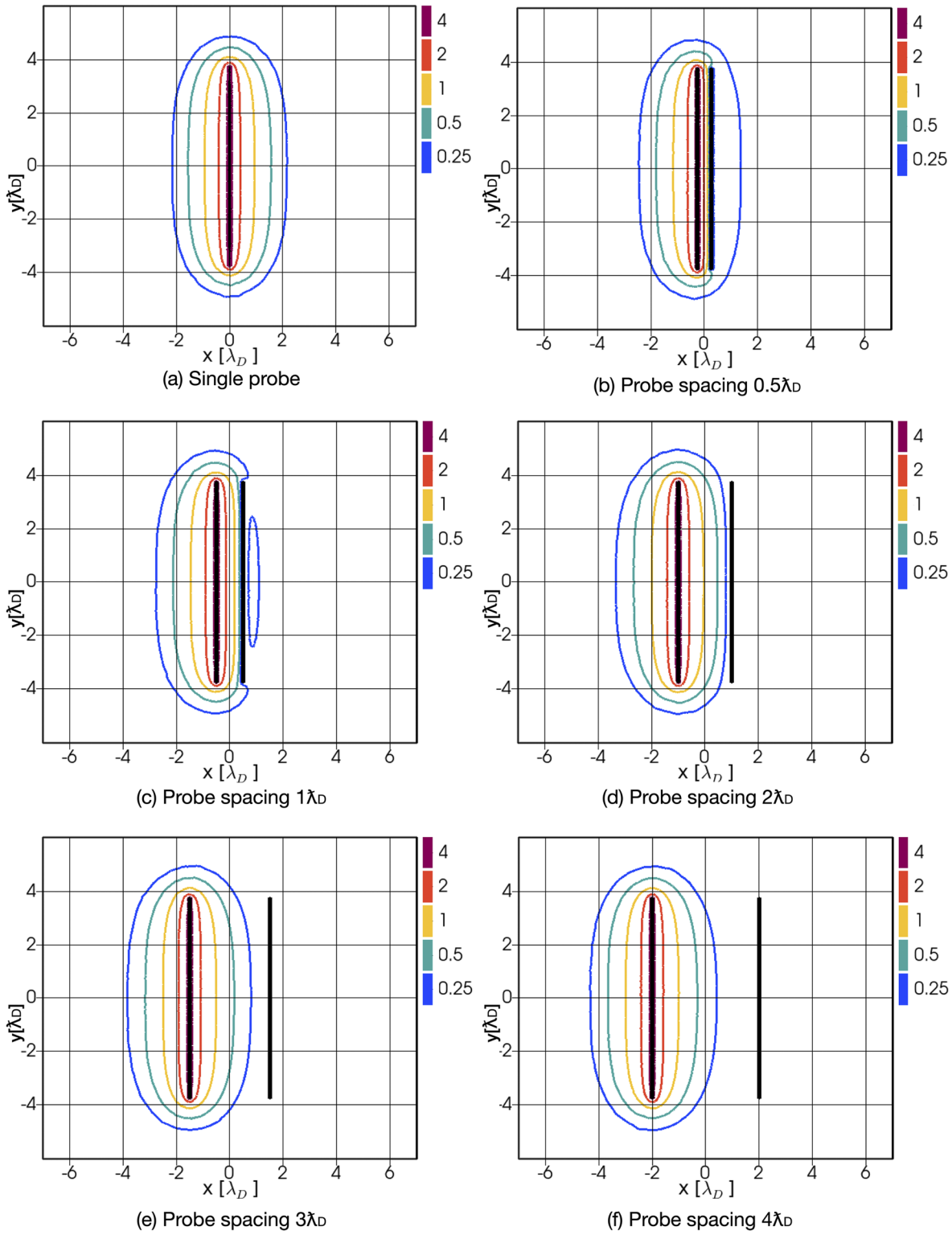

FIG. 8. Equipotential lines (V) in the sheath for the probe to the left biased at 5 V and to the right at 0 V. The spacing between the probes ranges from 0.5 to 4 Debye lengths. The density $n_i = n_e = 10^5$ cm^{-3}, and the temperature $T_i = T_e = 0.8$ eV.

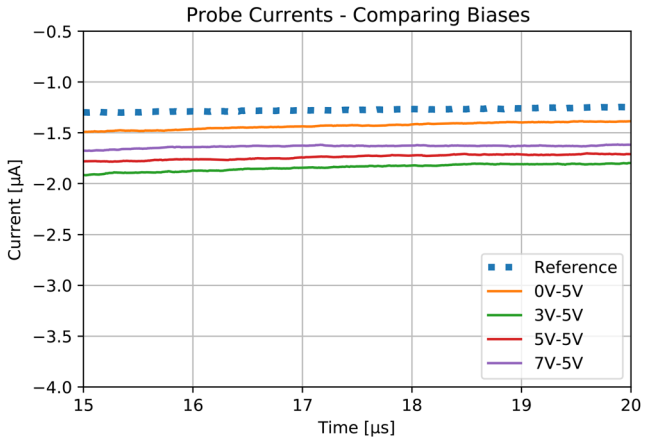

FIG. 9. Probe current at steady state for a probe biased at 5 V next to a probe biased at 0, 3, 5, and 7 V compared to the single reference probe at 7 V. The probe spacing is $\lambda_D = 2$.

and how it was affected by the distance between the probes and the applied probe bias. We started out by simulating one single probe biased at 0, 3, 5, or 7 V with respect to the ambient plasma. These results were used as a reference for the dual probe simulations. We then introduced the second probe. In this dual probe setup, the probes were arranged so that one probe had a fixed bias at 0 V and the other with a fixed bias at 3, 5, or 7 V. We repeated the simulations for various spacings between the probes, ranging from half the Debye length, $0.5\lambda_D$, up to four times the Debye length, $4\lambda_D$. To further investigate how the applied bias affected the current, we ran an additional set of simulations where the probe distance was fixed at $2\lambda_D$. We then changed the bias where one probe was fixed at 3, 5, or 7 V and the bias of the second probe was either 0, 3, 5, or 7 V.

V. SELECTED NUMERICAL RESULTS

When the simulations start, the applied bias acts like a step-function, and the system needs time to stabilize. In Fig. 4, we can see

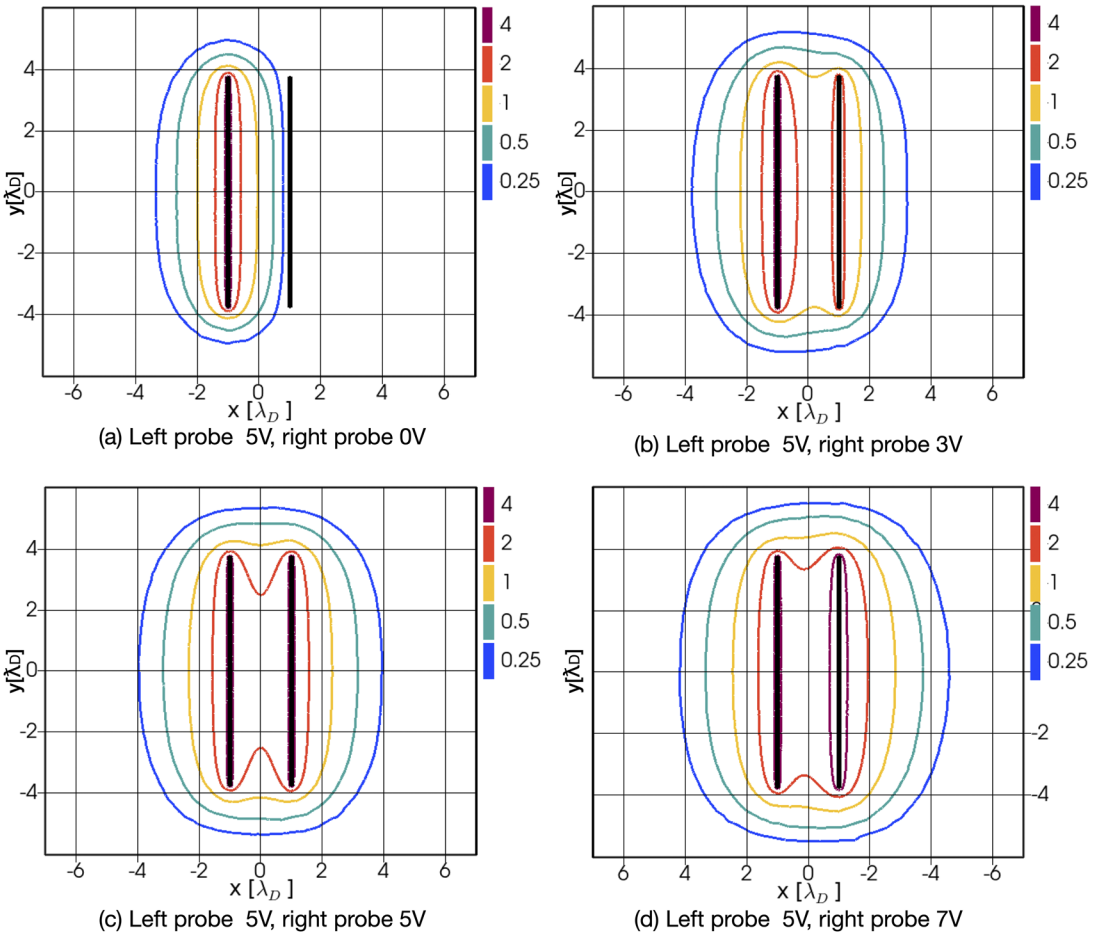

FIG. 10. Equipotential contours (V) in the vicinity of two cylindrical probes with respect to the ambient plasma. The spacing between the probes is fixed at two times the Debye lengths. The density $n_i = n_e = 10^5$ cm^{-3}, and the temperature $T_i = T_e = 0.8$ eV. The probe to the left has a fixed potential of 5 V, and the probe to the right is biased at 0, 3, 5, and 7 V.

that after about 1–2 μs, the current has a strong dip. This is because the electrons closest to the probe, where the electric field is strongest, are attracted to the probe. When most of these electrons are captured, the sheath starts to stabilize. From Fig. 4, we can see that the systems need at least 10 μs to stabilize. While the electrons, due to their lower mass than the ions, adapt rather fast, within a few electron plasma periods (Table II), the heavier ions need more time to reach steady state. The theoretical plasma period for the ion is 60.1 μs. However, we need to be aware that the simulation has been run with a speedup of 16 times, which is implemented as a reduction in the ion mass in the model. In Fig. 4, we can see oscillations with a period about 4–5 μs. Compensating for the speedup, we have an ion period of 64–80 μs, which is in the same range as the theoretical ion period. We can see that the relative deviation among the currents in Fig. 4 are relatively stable after about 15 μs. In the subsequently presented results of Figs. 5–7, we zoom in on the currents after the simulations have reached stable state from 15 to 20 μs. All presented currents were filtered with an exponential moving average filter with a relaxation time of 0.1 μs to reduce the noise. The currents presented in Tables III and IV were extracted from the filtered data and a mean value from the last ion period. In Figs. 8 and 9, we present equipotential plots for varying probe spacings and prob biase voltages. The probe spacings are all normalized to the Debye length.

A. Varying probe spacing

Figure 8 shows the electrostatic equipotential in the sheath around the probe at steady-state conditions at different distances between the probes. In Fig. 8(a), we see the sheaths for a single probe biased at 5 V, and in Figs. 8(b)–8(f), we see the same probe with a fixed bias at 5 V now placed next to a probe with a fixed bias at 0 V with $0.5\lambda_D$, $1\lambda_D$, $2\lambda_D$, $3\lambda_D$, and $4\lambda_D$ spacing between the probes. The corresponding currents can be seen in Fig. 6. Results from simulations with the same variations in probe spacing, but with probes with a combination of either 3–0 or 7–0 V bias, are shown in Figs. 5 and 7. The currents for the different spacings and probe biases were compared to the reference probe and are summarized in Table III together with the deviation from the reference probe.

B. Varying probe bias

Figure 10 shows the equipotential surrounding two cylindrical probes with a fixed spacing at $2\lambda_D$ between the probes and a varying bias. The one to the left has a fixed bias of 5 V, and probe to the right is now biased at 0, 3, 5, or 7 V. The corresponding currents can be seen in Fig. 9. Results from the same simulations with the left probes biased at 3 or 7 V are summarized in Table IV together with the deviation from the reference probe.

C. Double probes vs single probe

In Fig. 11, we compare currents for a double probe setup vs a single probe, where all probes have the same bias at 3, 5, or 7 V. The distance between the probes was fixed at two times the Debye length $2\lambda_D$ and a symmetrical setup with the same distance to the boundary for both probes. The equipotential surrounding two probes for the 5 V bias case can be seen in Fig. 10 and be compared to the equipotential for a single probe as presented in Fig. 8.

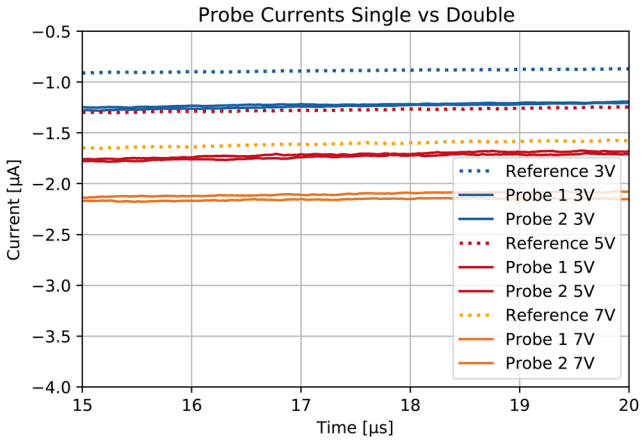

FIG. 11. Probe current for a single reference probe compared to a double probe setup biased at 3, 5, and 7 V. The probe spacing is $\lambda_D = 2$.

VI. DISCUSSION AND CONCLUSION

We can see from Fig. 8 that the equipotential is affected by introducing a second probe as well as the spacing between these probes. When the two probes are very close, as in Figs. 8(b)–8(d), where the probes are separated by $0.5\lambda_D$, $1\lambda_D$, and $2\lambda_D$, the equipotential lines are compressed between the probes, and the potential is reduced in space compared to the potential of a single reference probe. For $0.5\lambda_D$ and $1\lambda_D$, we can see that the two probes have a common sheath. However, for simulations with the $3\lambda_D$ spacing, we observe that the potential is comparable to the reference probe, and for the $4\lambda_D$ case, we can see that the potential is larger and slightly stretches out between the probes. This is most likely attributed to the lower density of electrons between the probes to equal the applied potential to the probes.[5] When we examine the corresponding currents listed in Table III, we observe that the currents are larger when the probes have smaller spacing. This deviation can be of significant value, for instance, it is close to 60% for the $0.5\lambda_D$ spacing, as seen in Table III. The current and the deviation compared to the reference probe are reduced as the spacing between the probes increases up to $3\lambda_D$. We would expect that when the distance between the probes is large enough, the current reaches the level of the reference probe, and it would stabilize at this level. However, we can see a small reduction in the current when the distance is larger than $3\lambda_D$. At these distances, the effect of the common field seems to vanish, and the reduction in the current compared to the reference probe is most likely caused by the lower density of electrons between the probes, as we also identified in the equipotential. We should also be aware that effects caused by differences in the generated mesh for each setup can occur. However, the deviation in current is small and within 0.7%–2.9% of the current of the reference probe and is marginal compared to the deviation when the probes are closer in space. The deviation is also less than the deviation between two identical probes, as seen in Fig. 11, where both probes were expected to have the same current. Thus, it is reasonable to say that the error is within the margin we expect for our simulations.

The applied bias voltage will also to a high degree affect the surrounding potential and the deviation of the measured currents. In

Fig. 10, where the distance between the probes is fixed at $2\lambda_D$, we can see how the equipotential lines stretch out and form a common field as the bias voltage of the second probe increases. This is also reflected in the corresponding currents in Table IV, all being significantly higher than the current of the single reference probe. We assume that this is caused by a common sheath that will attract more electrons. This is further supported by the results shown in Fig. 11 and in Table IV where we compare two probes separated by $2\lambda_D$, both with the same bias of 3, 5, or 7 V, all showing larger currents with a deviation of 36.9%, 35.0%, and 36.4%, respectively, than a single reference probe. It is also worth mentioning that for an *in situ* system, the spacecraft will collect the very same high mobility electron and thereby achieve a negative potential, forming a sheath. From our study, we can see how a thin charged probe affects the current of a nearby second probe, and accordingly, we might assume that a larger charged spacecraft will compromise the measured current to an even higher degree than a nearby probe.

PIC simulations have been carried out for different probe spacings and probe biases, and our results reveal that the probe spacing to a high degree will affect the probe current. In general, we can see that when the distance between the probes is small, less than $3\lambda_D$, we can expect an increase in the probe current. For a probe spacing larger than $3\lambda_D$, we have comparable results to the single reference probe. We can also see that for a dual probe setup, the deviation in current increases with the bias voltage, so both the probe spacing and the probe bias need to be taken into account when an m-NLP system is designed. However, a probe spacing of $3\lambda_D$ also produces comparable results to the single probe even when the bias voltage was increased to 7 V. This indicates that a probe spacing of $3\lambda_D$ should be sufficient for most practical space applications in the ionosphere.

ACKNOWLEDGMENTS

This work was supported by the 4DSpace Strategic Research Initiative at the University of Oslo. The simulations have been run at the Abel Cluster and the Sigma2 cluster, owned by the University of Oslo and Uninett/Sigma2. We would also like to thank Richard Marchand for making the PTetra model available.

DATA AVAILABILITY

The data that support the findings of this study are available from the corresponding author upon reasonable request.

REFERENCES

[1]H. Garrett, "The charging spacecraft surface," Rev. Geophys. **19**, 577, https://doi.org/10.1029/rg019i004p00577 (1981).
[2]E. C. Whipple, "Potentials of surfaces in space," Rep. Prog. Phys. **44**, 1197–1250 (1981).
[3]H. M. Mott-Smith and I. Langmuir, "The theory of collectors in gaseous discharges," Phys. Rev. **28**, 727–763 (1926).
[4]R. L. Boggess, L. H. Brace, and N. W. Spencer, "Langmuir probe measurements in the ionosphere," J. Geophys. Res. **64**, 1627–1630, https://doi.org/10.1029/jz064i010p01627 (1959).
[5]R. L. Merlino, "Understanding Langmuir probe current-voltage characteristics," Am. J. Phys. **75**, 1078–1085 (2007).
[6]R. B. Lobbia and A. D. Gallimore, "Temporal limits of a rapidly swept Langmuir probe," Phys. Plasmas **17**, 073502 (2010).
[7]K. S. Jacobsen, A. Pedersen, J. I. Moen, and T. A. Bekkeng, "A new Langmuir probe concept for rapid sampling of space plasma electron density," Meas. Sci. Technol. **21**, 085902 (2010).
[8]W. J. Miloch, "Wake effects and mach cones behind objects," Plasma Phys. Controlled Fusion **52**, 124004 (2010).
[9]H. Amemiya and G. Fuchs, "Range of application for asymmetric double probes," Jpn. J. Appl. Phys., Part 1 **30**, 3531–3532 (1991).
[10]P. Ludwig, W. J. Miloch, H. Kählert, and M. Bonitz, "On the wake structure in streaming complex plasmas," New J. Phys. **14**, 053016 (2012).
[11]H. Hoang, K. Røed, T. A. Bekkeng, J. I. Moen, A. Spicher, L. B. N. Clausen, W. J. Miloch, E. Trondsen, and A. Pedersen, "A study of data analysis techniques for the multi-needle Langmuir probe," Meas. Sci. Technol. **29**, 065906 (2018).
[12]S. Marholm and R. Marchand, "Finite-length effects on cylindrical Langmuir probes," Phys. Rev. Res. **2**, 023016 (2020).
[13]A. Barjatya and W. Merritt, "Error analysis of multi-needle Langmuir probe measurement technique," Rev. Sci. Instrum. **89**, 043507 (2018).
[14]T. A. Bekkeng, K. S. Jacobsen, J. K. Bekkeng, A. Pedersen, T. Lindem, J.-P. Lebreton, and J. I. Moen, "Design of a multi-needle Langmuir probe system," Meas. Sci. Technol. **21**, 085903 (2010).
[15]C. K. Birdsall, *Plasma Physics via Computer Simulation* (CRC Press, 1985).
[16]V. L. Rekaa, "Numerical simulations of kinetic plasmas," Ph.D. thesis, University of Oslo, Oslo, 2014.
[17]R. Marchand, "PTetra, a tool to simulate low orbit satellite–plasma interaction," IEEE Trans. Plasma Sci. **40**, 217–229 (2012).
[18]R. Marchand and P. A. Resendiz Lira, "Kinetic simulation of spacecraft–environment interaction," IEEE Trans. Plasma Sci. **45**, 535–554 (2017).
[19]C. Geuzaine and J.-F. Remacle, "Gmsh: A 3-D finite element mesh generator with built-in pre- and post-processing facilities," Int. J. Numer. Methods Eng. **79**, 1309–1331 (2009).
[20]C. K. Birdsall and N. Maron, "Plasma self-heating and saturation due to numerical instabilities," J. Comput. Phys. **36**, 1–19 (1980).
[21]H. Okuda, "Nonphysical noises and instabilities in plasma simulation due to a spatial grid," J. Comput. Phys. **10**, 475–486 (1972).